

3D pattern of brain abnormalities in Williams syndrome visualized using tensor-based morphometry

Ming-Chang Chiang,^a Allan L. Reiss,^b Agatha D. Lee,^a Ursula Bellugi,^c Albert M. Galaburda,^d Julie R. Korenberg,^e Debra L. Mills,^f Arthur W. Toga,^a and Paul M. Thompson^{a,*}

^aLaboratory of Neuro Imaging, Brain Mapping Division, Department of Neurology, UCLA School of Medicine, 635 Charles E. Young Drive South, Suite 225E, Los Angeles, CA 90095-7332, USA

^bCenter for Interdisciplinary Brain Sciences Research and Department of Psychiatry and Behavioral Sciences, Stanford University School of Medicine, Stanford, CA 94305, USA

^cSalk Institute Laboratory for Cognitive Neuroscience, La Jolla, CA 92037, USA

^dHarvard Medical School Department of Neurology, Boston, MA 02215, USA

^eCedars-Sinai Medical Center and UCLA Department of Pediatrics, Los Angeles, CA 90095, USA

^fEmory University Department of Psychology, Atlanta, GA 30322, USA

Received 6 January 2007; revised 29 March 2007; accepted 10 April 2007
Available online 20 April 2007

Williams syndrome (WS) is a neurodevelopmental disorder associated with deletion of ~20 contiguous genes in chromosome band 7q11.23. Individuals with WS exhibit mild to moderate mental retardation, but are relatively more proficient in specific language and musical abilities. We used tensor-based morphometry (TBM) to visualize the complex pattern of gray/white matter reductions in WS, based on fluid registration of structural brain images.

Methods: 3D T1-weighted brain MRIs of 41 WS subjects (age [mean ± SD]: 29.2 ± 9.2 years; 23F/18M) and 39 age-matched healthy controls (age: 27.5 ± 7.4 years; 23F/16M) were fluidly registered to a minimum deformation target. Fine-scale volumetric differences were mapped between diagnostic groups. Local regions were identified where regional structure volumes were associated with diagnosis, and with intelligence quotient (IQ) scores. Brain asymmetry was also mapped and compared between diagnostic groups.

Results: WS subjects exhibited widely distributed brain volume reductions (~10–15% reduction; $P < 0.0002$, permutation test). After adjusting for total brain volume, the frontal lobes, anterior cingulate, superior temporal gyrus, amygdala, fusiform gyrus and cerebellum were found to be relatively preserved in WS, but parietal and occipital lobes, thalamus and basal ganglia, and midbrain were disproportionately decreased in volume ($P < 0.0002$). These regional volumes also correlated positively with performance IQ in adult WS subjects (age ≥ 30 years, $P = 0.038$).

Conclusion: TBM facilitates 3D visualization of brain volume reductions in WS. Reduced parietal/occipital volumes may be associated with visuospatial deficits in WS. By contrast, frontal lobes, amygdala, and cingulate gyrus are relatively preserved or even enlarged, consistent with unusual affect regulation and language production in WS.

© 2007 Elsevier Inc. All rights reserved.

Introduction

Williams syndrome (WS) is a neurodevelopmental microdeletion disorder, resulting in characteristic cardiovascular abnormalities and typical facial features. WS is also an informative model for studying the linkage between genetic deficits and their neurobiological effects on the brain and behavior. The syndrome is associated with deletion of a 1–2 Mb contiguous genomic region containing about 25 genes in chromosome band 7q11.23, including the genes for elastin which has been implicated in congenital heart defects in persons with WS (Korenberg et al., 2000), such as septal defects or pulmonary/aortic stenosis. Neurobiologically, individuals with WS exhibit mild to moderate mental retardation and learning difficulties, yet there are nonetheless distinctive patterns of relative strengths and weaknesses. Individuals with WS are profoundly impaired in visuoconstructive spatial abilities, impaired in problem solving, but show relative strengths in language, particularly expressive language and face processing. In addition, individuals with WS tend to exhibit a characteristic personality that includes overfriendliness as well as the use of language for social purposes (Bellugi et al., 1999, 2001).

Such an imbalance in intellectual ability has been associated with an uneven pattern of relative deficits and excesses in the volume of specific brain regions. Volumetric studies have shown that the volume of the frontal lobes in WS is relatively preserved compared with individuals with Down syndrome or healthy controls (Jernigan et al., 1993; Reiss et al., 2000), but occipital and superior parietal cortices are disproportionately reduced in volume (Reiss et al., 2004; Eckert et al., 2005). Volumetric studies can be labor-intensive, and the spatial detail obtained is limited by the manual delineation of pre-selected regions of interest so it cannot visualize the profile of volume differences at the voxel-by-voxel level. Voxel-based morphometry (VBM) provides more spatial

* Corresponding author. Fax: +1 310 206 5518.

E-mail address: thompson@loni.ucla.edu (P.M. Thompson).

Available online on ScienceDirect (www.sciencedirect.com).

detail regarding the profile of tissue excess and deficits throughout the brain region, by comparing the gray matter density (smoothed gray matter maps) in spatially normalized MR images at each voxel. VBM studies have detected systematic differences in brain morphology between WS and normal subjects, such as reduced volumes in parieto-occipital cortex (Meyer-Lindenberg et al., 2004; Reiss et al., 2004; Boddaert et al., 2006; Eckert et al., 2006a). Nevertheless, these studies have often been based on small samples. Even so, effect sizes in VBM studies are typically small, and may be insufficient to describe morphological variations that may be broadly distributed throughout the entire brain in this neurodevelopmental disorder. More recent work has examined cortical gray matter thickness, using surface-based modeling and elastic warping of sulcal patterns to integrate information across subjects (Thompson et al., 2005). This work identified a circumscribed area of the right perisylvian and inferior temporal regions where the cortex was on average 5–10% thicker in Williams syndrome, suggesting a localized failure of cortical maturation. Other studies have detected temporo-parietal gyrification differences (Eckert et al., 2006b), and increased cortical complexity quantified using fractal dimension measures (Thompson et al., 2005), mean curvature maps (Gaser et al., 2006; Tosun et al., 2006, 2007), or by counting sulcal branches identified automatically as a graph of connected curves on the cortex (Shi et al., 2007).

In this paper, we apply tensor-based morphometry (TBM), see Davatzikos et al. (1996, 2001), Thompson et al. (2000), Fox et al. (2001), Shen and Davatzikos (2003), Chung et al. (2004), Studholme et al. (2004), and Chiang et al. (2007) for related work, to detect and automatically quantify subtle and distributed patterns of brain volume differences between 41 WS and 39 normal subjects. In the TBM approach, all images are nonlinearly deformed to match a preselected brain image, which acts as a template. Then, the Jacobian determinant (i.e., the local expansion factor) of the deformation fields is used to gauge the local volume differences between the individual images and the template, and these can be analyzed statistically to identify group differences or localized volume increases/reductions at the voxel level. In our implementation of TBM, which we have previously applied to examine brain atrophy in HIV/AIDS (Chiang et al., 2007), nonlinear image deformation is based on a fluid-deformation algorithm by maximizing the Jensen–Rényi divergence (JRD) of the joint intensity histogram (Chiang et al., 2007). Our results demonstrate that TBM may more clearly visualize the unique morphological profile in WS brains, identifying a more extensive but complementary pattern of differences relative to prior work using voxel-based morphometry or volumetric parcellation. Among adult WS subjects, we also examined links between volumes of specific brain regions and intellectual performance. Finally, we examine the distribution of brain volume asymmetry in both WS and control subjects, mapping the profile of group differences.

Methods

WS and control subjects

The study analyzed the data of 41 subjects with genetically confirmed Williams syndrome ([mean±SD]: 29.2±9.2 years of age; range 12–50 years of age; 18M/23F; diagnosis confirmed by fluorescent *in situ* hybridization tested for deletion of one copy of the elastin gene on chromosome 7) and 39 age-matched healthy

controls (27.5±7.4 years of age; range 18–49 years of age; 16M/23F). These subjects were included in Reiss et al. (2004); the same cohort was studied in our prior reports (Thompson et al., 2005; Gaser et al., 2006), but in this study we excluded one WS and one control subject whose scans had relatively poor image contrast. Given the large effect sizes and relatively large sample, we preferred to exclude these two scans, as the sample size was more than sufficient to model the effects of interest. Nevertheless, the age distribution (mean, SD, and range) of the subjects in this paper is almost identical to that in Thompson et al. (2005) and Gaser et al. (2006) (WS [mean±SD]: 29.2±9.0 years of age; range 12–50 years of age; 19M/23F; controls: 27.5±7.4 years of age; range 18–49 years of age; 16M/24F). Exclusion criteria included a history of medical conditions not typically associated with WS, such as epilepsy or other neurological conditions. All WS participants were evaluated at the Salk Institute (La Jolla, CA) as part of a program project on genetics, neuroanatomy, neurophysiology, and cognition. Wechsler intelligence quotient (IQ) scores (full-scale, verbal, and performance) were available for 39 of the 41 WS subjects; the two untested subjects exhibited similar levels of cognitive function on other measures. As in the study by Reiss et al. (2004), healthy control subjects (with no history of major psychiatric, neurological, or cognitive impairment) were recruited at both the Salk Institute and Stanford University. Control subjects were further screened to rule out any history of learning, language, or behavioral disorder. The majority of controls in the study did not have IQ testing performed. All procedures were approved by the Institutional Review Boards of both institutions, and all participants provided informed consent (and parents or guardians provided written consent where appropriate).

Image scanning and registration

Image acquisition and registration

All participants received 3D spoiled gradient recovery (SPGR) anatomical brain MRI scans (256×192×124 matrix, TR=24 ms, TE=5 ms; 24-cm field of view; 1.2-mm slices, zero gap; flip angle=45°) using a GE-Signa 1.5 T scanner (General Electric, Milwaukee, MI). The same scanner type and exactly the same SPGR pulse sequence were used at the Salk Institute and at Stanford University. Following removal of extracerebral tissues (e.g., scalp and meninges), the MRI brain scan of each subject was co-registered to the ICBM53 average brain template (Mazziotta et al., 2001) using 9-parameter affine registration with translations, rotations, and independent scalings in the *x*-, *y*-, and *z*-directions. The template is one of several standardized adult brain templates and was generated by averaging high-resolution brain MRI scans (*n*=53) in the ICBM standard space to improve the signal-to-noise ratio, after nonlinear image registration using the ANIMAL algorithm (Collins et al., 1995; Montreal Neurological Institute, McGill University, Canada); the template is part of the MINC distribution of brain templates, image analysis algorithms and display software. To retain information on the overall change in brain volume incurred by scaling images from scanner space to the ICBM space (see below), a zoom factor was computed from the determinant of the global linear transformation.

All subjects' images were then registered to an optimized target (see below for target selection) using a nonlinear algorithm based on maximizing the Jensen–Rényi divergence (JRD) of the joint intensity histogram, with the deformation field regularized in a fluid scheme (Chiang et al., 2007).

Target selection

To select an optimized target, we adopted the “minimum-deformation target” (MDT) proposed by Kochunov et al. (2001). For subject image i ($1 \leq i \leq n$) initially serving as a registration target, a target quality score (TQS), summarizing its deviation from all the other images, is given by:

$$\text{TQS}_i = \frac{1}{N} \sum_{k=1}^N \left[\sqrt{S_i(\mathbf{x}_k) \cdot D_i(\mathbf{x}_k)^{\frac{1}{2}}} \right]$$

where $\mathbf{x}_k \in \text{GM, WM or CSF}$, $1 \leq k \leq N$

$$\bar{\mathbf{u}}_i(\mathbf{x}) = \frac{1}{n} \sum_{j=1, j \neq i}^n \mathbf{u}_j(\mathbf{x})$$

$$S_i(\mathbf{x}) = \|\bar{\mathbf{u}}_i(\mathbf{x})\|,$$

$$D_i(\mathbf{x}) = \frac{\sum_{j=1, j \neq i}^n \|\mathbf{u}_j(\mathbf{x}) - \bar{\mathbf{u}}_i(\mathbf{x})\|^2}{n-2}. \quad (1)$$

At each voxel, S and D were computed from the deformation fields mapping all other subjects to the target (with \mathbf{u}_j denoting the deformation vector for subject j) fluidly mapped to the target by maximizing the Jensen–Rényi divergence (Chiang et al., 2007). The subject with the lowest TQS was then defined as the best individual target (BIT), denoted by I_{BIT} , then the MDT brain (I_{MDT}) is defined by:

$$I_{\text{MDT}}(\mathbf{x}) = I_{\text{BIT}}(\bar{\mathbf{h}}^{-1}(\mathbf{x})), \quad (2)$$

where $\bar{\mathbf{h}}(\mathbf{x}) = \mathbf{x} - \frac{1}{n} \sum_{j=1}^n \mathbf{u}_j(\mathbf{x})$ is the average displacement field for all the other subjects mapped to the BIT, and $\bar{\mathbf{h}}^{-1}(\mathbf{x})$ was obtained from $\bar{\mathbf{h}}(\mathbf{x})$ following the iterative method in Christensen and Johnson (2001). We preferred the optimized target computed from the average transformation for a typical image (e.g., the BIT) rather than building a multi-subject average intensity atlas, as the former has sharper features and, in general, leads to larger effect sizes when used in a morphometric study (Christensen et al., 2006; Chiang et al., 2007). The MDT method is closest to what proposed in Christensen et al. (2006) and Park et al. (2003). Other template optimization methods (Avants and Gee, 2004; Joshi et al., 2004; Studholme and Cardenas, 2004; Twining et al., 2005) are also possible.

Tensor-based morphometry and statistical comparisons

Comparison of regional brain volumes between WS subjects and controls

The Jacobian tensor in the ICBM space was obtained by taking the spatial gradient of the deformation field from the fluid registration. Then the determinant of the Jacobian tensor in the native space (i.e. before the brain was affinely registered to the ICBM53 template), denoted by J_{native} , was computed from the Jacobian determinant in the ICBM space (J_{ICBM}) using $J_{\text{native}} = J_{\text{ICBM}} / \text{zoom factor}$, where the zoom factor was defined

in the previous section. The determinant of the Jacobian tensor was used as a local index of tissue expansion (Jacobian > 1) or shrinkage (Jacobian < 1) relative to the target (Davatzikos et al., 1996; Chung et al., 2001). The percentage difference in mean volume at each voxel was estimated from the ratio of the mean J_{native} in WS versus control subjects. This indicates the degree to which the volume of a specific region is higher or lower in WS than in matched controls, and the ratio can be turned into a percentage deficit. The Jacobian determinant values were first subjected to a log transformation because the null distribution of the log(Jacobian) is closer to Normal than that of the Jacobian determinant, which is skewed and bounded below by zero (Ashburner and Friston, 2000; Woods, 2003; Arsigny et al., 2005; Avants et al., 2006); see Leow et al. (2005, 2006) for a detailed analysis of the effects of log-transformation on the Jacobian distribution. We tested the significance of difference between the mean log(J_{native}) of the WS and control groups using the Mann–Whitney U test voxelwise. Since the total brain volume in WS subjects is less than that in control subjects (see Results), the difference of the mean log(J_{ICBM}) between the two groups was also compared by the Mann–Whitney U test, after the global brain volume differences had been adjusted out by transformation to the ICBM space. Furthermore, to detrend any possible confounding effect of subjects’ age, analysis of covariance (ANCOVA) was performed at each voxel, with each participant’s age treated as a covariate, from which we derived a percentage volume difference map adjusted for subjects’ age and the total brain volume (see Appendix A for details).

Correlations of regional brain volume with IQ scores

Spearman’s rank test was applied at each voxel to identify regions where regional brain volume (J_{native}) correlated with verbal or performance IQ in WS ($n=39$) and control ($n=16$) subjects separately. As the regions showing volumetric correlations with IQ may be different in different age groups (Shaw et al., 2006), we further divided the WS subjects into adolescents (range 12–16.9 years, $n=2$), young adults (range 17–29.9 years, $n=19$), and those in middle-adulthood (age ≥ 30 years, $n=18$), such that the number of subjects in the two adult groups was roughly equal, and tested the IQ correlations in the latter two groups. (There were too few control subjects with IQ scores available to allow comparable subdivisions for the controls.)

Brain asymmetry

We followed the method proposed by Park et al. (2004), where brain asymmetry was detected by mapping all the subjects to a symmetric brain template, and then regional volume differences between left and right hemispheres can be identified by comparing the Jacobian determinant at corresponding voxels in each hemisphere. Briefly, if $\mathbf{h}(\mathbf{x}) = \mathbf{x} - \mathbf{u}(\mathbf{x})$ is the displacement field for the MDT $I_{\text{MDT}}(\mathbf{x})$ mapped to its flipped image (across the midsagittal plane) $I_{\text{MDT}}(\mathbf{x})$, and $R(\mathbf{x})$ is the deformed image, i.e. $R(\mathbf{x}) = I_{\text{MDT}}(\mathbf{h}(\mathbf{x}))$, then with $\bar{S}(\mathbf{x}) = \frac{[R(\mathbf{x}) + I_{\text{MDT}}(\mathbf{x})]}{2}$, the symmetric template $S(\mathbf{x})$ is given by $S(\mathbf{x}) = \bar{S}(\bar{\mathbf{h}}^{-1}(\mathbf{x}))$, where $\bar{\mathbf{h}}^{-1}(\mathbf{x})$ is the inverse of $\bar{\mathbf{h}}(\mathbf{x})$, and $\bar{\mathbf{h}}(\mathbf{x}) = \mathbf{x} - \frac{\mathbf{u}(\mathbf{x})}{2}$. We then registered all the brains to the symmetric template $S(\mathbf{x})$ using the fluid JRD algorithm, and the difference between log(J_{ICBM}) between corresponding voxels (which are mirror images of each other with respect to the midsagittal plane) in the left and right

hemispheres of the symmetric template brain was compared using the Wilcoxon signed rank test, using two separate one-tailed tests for right hemisphere volume greater than left one and vice versa (this is appropriate, as the literature on hemispheric petalia – reviewed in Toga and Thompson (2003) – leads to pre-existing one-tailed hypotheses regarding normal frontal lobe volumetric excess on the right and occipital lobe excess in the left hemisphere). We also evaluated if there was any difference in degree of asymmetry between WS and control groups, using repeated measures analysis of variance (ANOVA) to test the group \times side interaction, with diagnosis (WS vs. control) as the between-subject factor, and side (left vs. right) as the within-subject factor (Carrion et al., 2001) (see Appendix B for details).

Statistical procedures for correction of multiple comparisons

Overall significance was assessed by permutation methods (Nichols and Holmes, 2001) to correct for multiple comparisons. Statistical testing was performed on each random permutation of subjects' labels (e.g. "disease" or "control" in Mann–Whitney U tests, IQ scores in the correlation tests, or the ordering of "left" and "right" in the Wilcoxon signed rank test) to construct a null distribution for the number of voxels more significant than a fixed primary threshold applied at the voxel level (here set to $P=0.01$). The omnibus probability (i.e., corrected for multiple comparisons) was determined by comparing the number of suprathreshold voxels in the true labeling to the permutation distribution. The number of permutations N was chosen to control the standard error SE_p of omnibus probability P , which follows a binomial distribution $B(N, P)$ with $SE_p = \sqrt{p(1-p)/N}$ (Edgington, 1995). We selected $N=8000$ tests out of the total number of possible permutations ($\approx 10^{23}$) such that the approximate margin of error (95% confidence interval) for P was around 5% of P , and 0.05 was chosen as the significance level.

For stronger control over the likelihood of false rejections of the null hypotheses with multiple comparisons, we adopted the method by Storey (2002), which directly measures the positive false discovery rate (p_{FDR}) under a given primary threshold. The p_{FDR} method is more powerful than the popular sequential p -value FDR method (Benjamini and Hochberg, 1995; Genovese et al., 2002), as it estimates the probability that the null hypothesis is true, from the empirical distribution of observed p -values (Manly et al., 2004). The p_{FDR} measure is theoretically more suitable for representing the "rate at which discoveries are false" than the FDR measure when the primary rejection region is relatively small (Storey, 2002). Briefly, p_{FDR} is the false discovery rate conditioned on the

event that positive findings, rejecting the null hypothesis, have occurred, and is given by

$$p_{FDR}(\gamma) = \frac{\pi_0 \Pr(P \leq \gamma | H = 0)}{\Pr(P \leq \gamma)}, \quad (3)$$

where $\pi_0 = \Pr(H=0)$ is the probability that the null hypothesis is true, and γ is the rejection threshold for the individual hypothesis, which was set to 0.01 in our experiments. We refer readers to Storey and Tibshirani (2001) and Storey (2002) for details of the estimation procedures to obtain p_{FDR} for statistical maps. By convention, a statistical map with $p_{FDR} < 0.05$, i.e. a false discovery rate less than 5%, was considered to be significant.

Permutation tests and p_{FDR} measures were performed on combined gray and white matter masks to generate P values that were corrected for multiple comparisons within regions containing brain tissue. White matter and gray matter masks were automatically segmented using an unsupervised Gaussian mixture classifier, after adjusting for spatial intensity inhomogeneity, using the software package "BrainSuite" (Shattuck and Leahy, 2002).

Results

Target selection and symmetric brain template

Fig. 1 shows brain MR images with lowest and highest TQS, the MDT, and the symmetric template. TQS is a measure of how much each brain deviates from all the others in the sample (including WS and controls), and there was no difference in TQS between WS and control subjects (WS: 2.48 ± 0.19 voxels, ranging from 2.23 to 2.88 voxels; controls: 2.45 ± 0.20 voxels, ranging from 2.12 to 2.97 voxels; $P=0.3$ for a group difference). The BIT happened to be one of the control subjects (TQS=2.12 voxels). The TQS of the MDT was 1.48 voxels.

Visualization of the profile of volume alterations in WS

The total brain volume was 13% smaller in WS than control subjects (WS: 925.65 ± 76.26 cm³; controls: 1062.54 ± 115.95 cm³; $P < 0.001$). This is apparent in the volume (percentage reduction) map comparing the group differences of J_{native} in Fig. 2, where WS subjects exhibited widespread volume reduction over the whole brain (permutation test $P < 0.0002$, $p_{FDR} = 0.0002$). To control for this overall difference in total brain volume between groups, J_{ICBM}

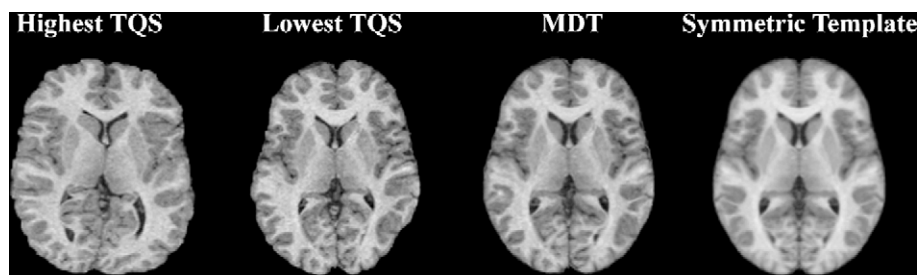


Fig. 1. This figure shows, from left to right, the brain with highest TQS (a WS subject), the lowest TQS (a control subject), the MDT, and the symmetric template derived from the MDT. The mean deformation distance between the registration target and the population of WS and control brains is greatly reduced by averaging the deformation fields, and the MDT, compared with the lowest TQS brain from which it is derived, has a smoother gyral morphology, and is close to symmetric.

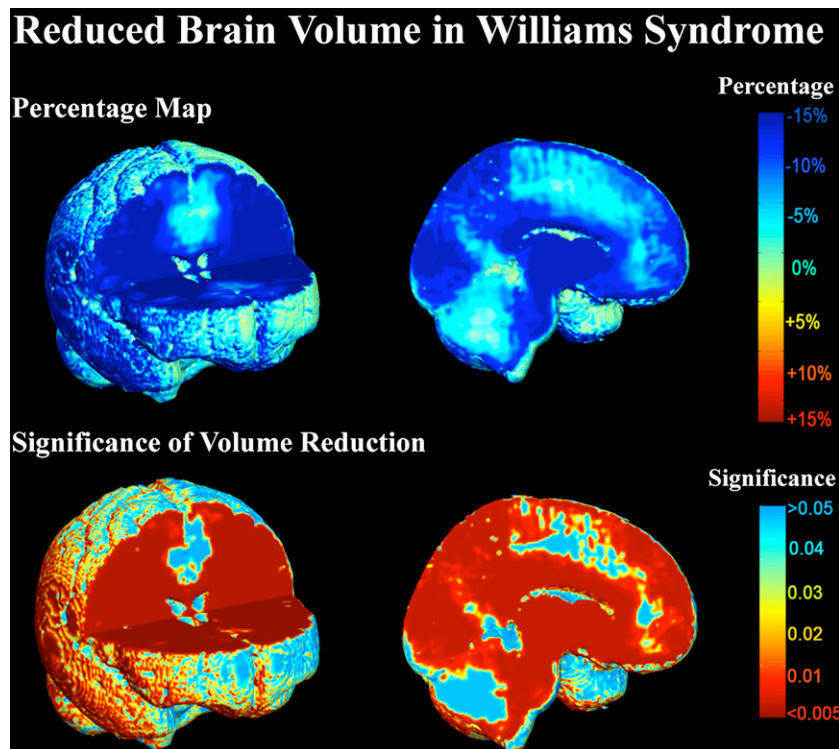


Fig. 2. Voxelwise comparisons of WS and control brain volumes in the native space show widespread volume reductions throughout the entire brain, which reflects the fact that total brain volume in WS subjects is less than controls. Nevertheless, the volumes of the frontal lobes and cerebellum are relatively preserved.

was compared voxelwise. Fig. 3 shows that, in WS subjects, the volume of prefrontal and orbito-frontal areas, the anterior cingulate gyrus, inferior parietal regions at the parieto-occipital junction, the superior temporal gyrus, amygdala and part of the hippocampus (most prominently on the right side), fusiform gyrus, and cerebellum were relatively preserved (which is represented as an ‘increase’ or ‘relative excess’ in the volume percentage maps; permutation test $P < 0.0002$, $p_{\text{FDR}} = 0.01$). However, occipital areas, parietal lobe regions close to the temporo-parietal junction, the splenium and posterior body of the corpus callosum, thalamus and basal ganglia (including globus pallidus, putamen, and caudate nucleus), and midbrain were disproportionately reduced in WS, i.e. reduced to an even greater extent than the level of overall brain volume reduction (permutation test $P < 0.0002$, $p_{\text{FDR}} = 0.01$). The volume increase/reduction in the native and the ICBM spaces was also found to be significant after adjusting for effects of age using ANCOVA (native space: permutation test $P < 0.0002$, $p_{\text{FDR}} = 0.03$; ICBM space: permutation test $P < 0.0002$, $p_{\text{FDR}} = 0.02$).

Correlations of regional brain volume with IQ scores

39 WS and 16 control subjects underwent IQ testing. WS subjects had lower full-scale, verbal and performance IQ scores than control subjects (full-scale IQ [mean \pm SD]: 68.7 \pm 8.4 vs. 104.3 \pm 12.4, $P < 0.001$; verbal IQ: 72.1 \pm 7.4 vs. 103.3 \pm 11.0, $P < 0.001$; performance IQ: 67.7 \pm 8.6 vs. 104.6 \pm 12.7, $P < 0.001$; Mann–Whitney U tests). However, WS subjects were relatively proficient in verbal tests as the difference between verbal and performance IQ scores was larger in WS (verbal–performance IQ:

4.4 \pm 7.1 in WS vs. –1.25 \pm 9.2 in controls, $P = 0.02$; Mann–Whitney U tests). This trend was made clearer by comparing the index (verbal–performance IQ)/0.5(verbal+performance IQ) to adjust for the group differences in IQ scores (WS: 0.066 \pm 0.099, controls: –0.011 \pm 0.084, $P = 0.005$; Mann–Whitney U tests). In either group, there were no positive or negative correlations between either verbal or performance IQ scores and the overall brain volume (in WS: $P = 0.90$ for verbal IQ, and $P = 0.56$ for performance IQ; in controls: $P = 0.09$ for verbal IQ, and $P = 0.11$ for performance IQ) or the regional brain volume (in the native space) (in WS: permutation test $P = 0.5$, $p_{\text{FDR}} = 1.0$ for verbal IQ, permutation test $P = 0.2$, $p_{\text{FDR}} = 0.28$ for performance IQ; in controls: permutation test $P = 0.07$, $p_{\text{FDR}} = 0.06$ for verbal IQ, permutation test $P = 0.09$, $p_{\text{FDR}} = 0.10$ for performance IQ; figures not shown).

We further examined IQ correlations with brain morphology in the adult WS subjects, classifying them into individuals in young adulthood (range 17–29.9 years, $n = 19$) or middle adulthood (age \geq 30 years, $n = 18$). There was no difference in verbal IQ between these two groupings (young-adult: 72.6 \pm 5.7, middle-adult: 73.1 \pm 7.9, $P = 0.96$; Mann–Whitney U tests), but the middle-adult individuals had higher performance IQ scores than the young-adult ones (middle-adult: 71.3 \pm 8.0, young-adult: 66.2 \pm 6.5, $P = 0.026$; Mann–Whitney U tests). Furthermore, in WS subjects aged 30 or over, regional brain volumes were positively correlated with performance IQ scores in bilateral anterior cingulate gyrus, in the genu and splenium of the corpus callosum, in parietal, occipital and prefrontal areas, right amygdala, hippocampus, fusiform gyrus and orbito-frontal areas, left superior temporal gyrus, and in the cerebellum and pons (permutation test: $P = 0.038$, $p_{\text{FDR}} = 0.02$, Fig. 4). Negative correlations were not significant. No positive or

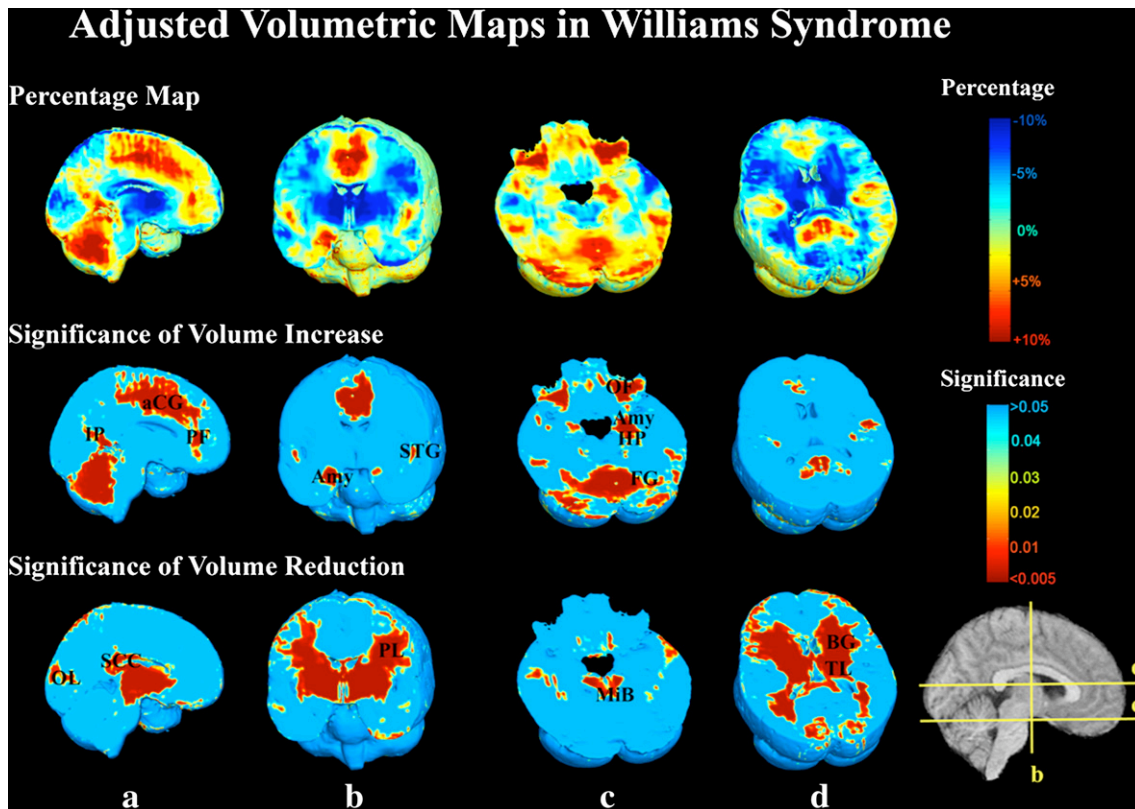


Fig. 3. Volumetric maps show systematic differences in brain morphology in WS. WS and control brain volumes were compared in the ICBM space to adjust for individual differences in total brain volumes. The ratio of the mean J_{ICBM} in WS to the mean J_{ICBM} in control subjects was computed voxelwise to map the 3D profile of brain volume increases (color-coded as red) or reductions (color-coded as blue) (first row). Panels (a) to (d) show relative preservation of the volume (which is shown as increase in the volume percentage maps) in prefrontal and orbito-frontal areas, anterior cingulate gyrus, inferior parietal regions at the parieto-occipital junction, superior temporal gyrus, amygdala and part of hippocampus (especially on the right side), fusiform gyrus, and cerebellum. Occipital areas, parietal lobes close to temporo-parietal junction, splenium and posterior body of the corpus callosum, thalamus and the basal ganglia (including globus pallidus, putamen, and caudate nucleus), and midbrain are disproportionately reduced. The Mann–Whitney U test was used to obtain the significance maps for the volume increase (second row) or reduction (third row). Abbreviations: aCG: anterior cingulate gyrus, Amy: amygdala, BG: basal ganglia, FG: fusiform gyrus, HP: hippocampus, IP: inferior parietal region, MiB: midbrain, OF: orbito-frontal area, OL: occipital lobe, PF: prefrontal area, PL: parietal lobe, SCC: splenium of the corpus callosum, STG: superior temporal gyrus, TL: thalamus.

negative correlations were detected between regional brain volume and verbal IQ scores in healthy control adults aged 30 or over, and verbal and performance IQ scores in WS subjects younger than 30 (figures not shown).

Brain asymmetry in WS and control subjects

Fig. 5 shows that the patterns of brain volume asymmetry are similar for both WS and control groups (brain volume asymmetry was significant in both WS and control groups, corrected for multiple comparisons, with permutation test $P < 0.0002$, $p_{FDR} = 0.013$ for regions with right > left volumes and permutation test $P = 0.0008$, $p_{FDR} = 0.017$ for regions with left > right volumes in WS, and permutation test $P = 0.005$, $p_{FDR} = 0.013$ for right > left and permutation test $P = 0.001$, $p_{FDR} = 0.015$ for left > right in controls). As anticipated from the literature on brain torque and hemispheric petalias (Toga and Thompson, 2003), there was a rightward asymmetry (i.e., greater volume on the right) in the frontal and temporal lobes, and leftward asymmetry in occipital lobes. The thalamus, putamen, globus pallidus, and caudate nucleus were found to be larger on the left side in both groups. WS subjects had a right larger than left planum temporale. In control subjects,

the planum temporale is larger in the left hemisphere, but the difference was either at trend-level or only significant for the medial part. WS subjects also differed from controls in that they displayed a rightward asymmetry in amygdala and hippocampus, and exhibited a less prominent occipital petalia. However, this group \times side interaction does not reach statistical significance, when corrected for multiple comparisons ($p_{FDR} = 0.9$).

Scanner effect

78 subjects were scanned at the Salk Institute (with 24 WS and 16 controls at one scanner, and 17 WS and 21 controls at the other scanner), and 2 subjects were scanned at Stanford University (both were controls), using the same GE-Signa 1.5 T scanner type and the same SPGR pulse sequence. For the subjects imaged at the Salk Institute, there was no difference in the distributions of diagnosis (*chi-square test*: $P = 0.257$), age ([mean \pm SD] 28.4 ± 8.6 vs. 28.4 ± 8.2 , $P = 0.987$), or gender (14M/26F vs. 18M/20F, $P = 0.358$) between those who were assigned to each of the two scanners. We further covaried out the scanner effect from the volumetric results by comparing J_{ICBM} and J_{native} (the ICBM space and native space Jacobian maps) between WS and control subjects using ANCOVA,

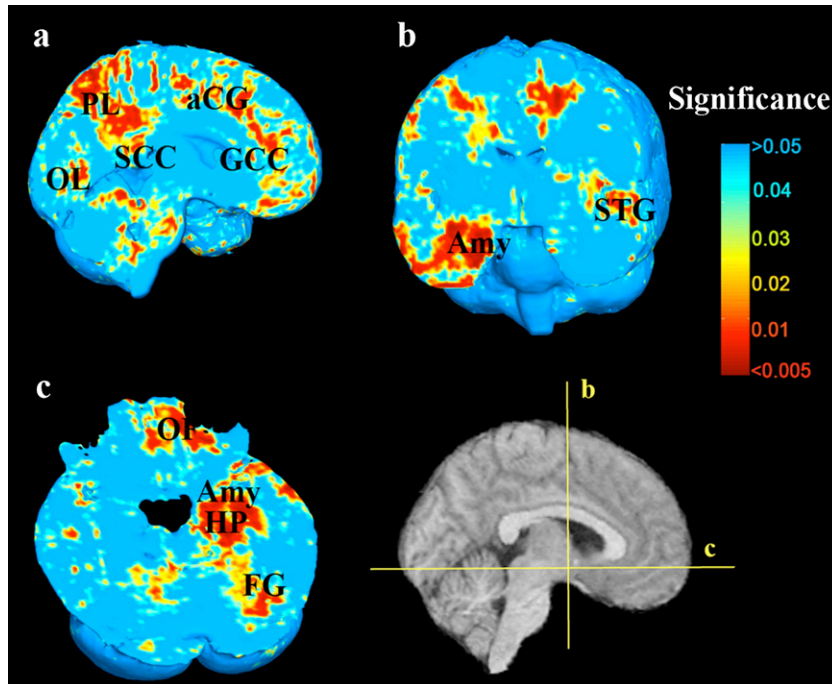


Fig. 4. In WS subjects aged 30 or over, regionally greater brain volume was associated with higher performance IQ scores in (a) bilateral anterior cingulate gyrus, in the genu and splenium of the corpus callosum, parietal, occipital and prefrontal areas, and in the cerebellum and pons (b) left superior temporal gyrus and (c) right amygdala, hippocampus and orbito-frontal areas. These correlations were assessed using Spearman's (non-parametric) rank correlation. Abbreviations: aCG: anterior cingulate gyrus, Amy: amygdala, FG: fusiform gyrus, GCC: genu of the corpus callosum, HP: hippocampus, OF: orbito-frontal area, OL: occipital lobe, PL: parietal lobe, SCC: splenium of the corpus callosum, STG: superior temporal gyrus.

with the scanner treated as a confounding variable (the two scanners at the Salk Institute were coded as 1 and 2, respectively, and the scanner at Stanford University as 3). We found that volume increase/reduction in the native and the ICBM spaces was still highly significant in the presence of the scanner covariate (native space: permutation test $P < 0.0002$, $p_{\text{FDR}} = 0.0008$; ICBM space: permutation test $P < 0.0002$, $p_{\text{FDR}} = 0.018$).

Discussion

Our study demonstrated that TBM based on fluid registration is helpful to visualize the profile of 3D volumetric differences in WS. Our findings corroborate prior work that used VBM and volumetric assessments (Reiss et al., 2000, 2004; Schmitt et al., 2001a,b; Tomaiuolo et al., 2002; Meyer-Lindenberg et al., 2004, 2005b; Boddaert et al., 2006; Eckert et al., 2006a), showing disproportionate reduction in parieto-occipital lobes, posterior corpus callosum, thalamus and midbrain, but preservation in prefrontal and orbito-frontal areas, anterior cingulate, superior temporal gyrus, amygdala and hippocampus, fusiform gyrus and cerebellum. Reduction in the volume of the parieto-occipital regions, as well as the posterior corpus callosum where white matter fibers interconnect opposite visual and visual association cortices (De Lacoste et al., 1985), may be causally implicated in the visuospatial dysfunction observed in WS subjects (Bellugi et al., 1999, 2000; Brown et al., 2003). Relative preservation of the right fusiform gyrus and amygdala, which are involved in visual analysis of faces among other tasks (Haxby et al., 1999; Kawashima et al., 1999; Hoffman and Haxby, 2000; Mobbs et al., 2004; Meyer-Lindenberg et al., 2005a; Haxby, 2006), may be

linked to the near-normal level of face perception and recognition in WS subjects (Bellugi et al., 2000). The right amygdala was also found to be more active in WS subjects than controls in response to musical stimuli, which may be relevant to their exceptional sensitivity to music (Levitin et al., 2003). Reductions in the basal ganglia in WS have not been emphasized in prior studies. Jernigan et al. (1993) found that, based on MR volumetry, the lenticular nucleus to cerebral gray matter proportion is smaller in WS compared with Down syndrome, but is not different than in controls. Reiss et al. (2004) detected a single cluster with reduced gray matter density in the left caudate nucleus by applying VBM. Using TBM here, we showed that the basal ganglia, including the caudate nucleus, putamen and globus pallidus, are significantly reduced in WS. This is congruent with a recent functional MRI study (Mobbs et al., 2006), which showed that neural activity in bilateral striatum, especially in the caudate nucleus and putamen, is significantly lower in WS than in typically developing subjects during a response inhibition task, suggesting striatal dysfunction. Although TBM is based on using a deformation algorithm to infer local volume increase or decrease based on changes in tissue boundaries, rather than true changes in cell/fiber density or physiological integrity of neural tissues, it is sensitive enough to visualize structural abnormalities that may be linked with these functional alterations.

The WS and control subjects were examined in Reiss et al. (2004), Thompson et al. (2005), and Gaser et al. (2006); however, this paper is partially independent of the previous ones in both the methodologies and in regions and signals assessed. Reiss et al. (2004) compared total and regional gray and white matter volume and density using volumetric measurements and the VBM method.

Thompson et al. (2005) identified regionally specific alterations in cortical thickness, using surface-based cortical models and sulcal landmark-guided registration. This paper uses the TBM method, which focuses mainly on mapping the 3D profile of volume reductions in subcortical gray and white matter in WS. As such, while our results are largely congruent with earlier findings of subcortical volume reductions, they should be viewed as presenting complementary measures; the study cannot strictly speaking be viewed as an independent replication of earlier reports as the sample of subjects assessed is the same.

If cortical gray matter distribution is compared across subjects, clearly the geometry of the gyri and sulcal features is highly convoluted and individual gyri or sulci are not readily distinguished based on image intensity alone. As a result, most intensity-based automated registration algorithms (for both TBM and VBM) are unable to match them accurately for purposes of morphometric comparisons, unless specific cortical features are added to constrain the correspondence (e.g., Fischl et al., 1999; Thompson et al., 2000). In particular, a surface-based warping method, using explicitly defined cortical landmarks, may be more appropriate for detecting cortical thickening or thinning in WS, as landmark points defined on the cortical surfaces can be explicitly matched when compared data across subjects and groups (Thompson et al., 1996, 2005). Nevertheless, surface-based warping methods provide no information below the cortex; manual labeling of gyral and sulcal landmarks can also be labor-intensive. If anatomical correspondences are defined automatically to increase efficiency, algorithms typically assume that aligning 3D features, such as mean curvature or conformal factor measures, increases anatomical homology across subjects (Fischl et al., 1999; Wang et al., 2005; Lui et al., 2007). Therefore, cortical differences in WS may be better detected using surface-based modeling methods, but TBM complements traditional volumetric studies in WS with greater automation, additional detail in the form of 3D maps, and improved 3D visualization of deficits in subcortical gray and white matter regions.

Compared with the unmodulated (Reiss et al., 2004; Boddaert et al., 2006) or modulated (Meyer-Lindenberg et al., 2004; Eckert et al., 2006a) VBM methods, in which the “gray matter density” or “gray matter volume” is compared across groups of subjects, the TBM method directly detects volume reductions in gray and white matter. Because VBM and TBM differ in the signals they examine, and in their power to detect differences in different regions of the brain, there are some differences in volumetric findings using these methods. Specifically, our TBM results here are consistent with those found by Reiss et al. (2004) using unmodulated VBM, in that gray matter volume (TBM) or density (unmodulated VBM) was reduced in parietal–occipital gyri, but preserved in orbito-frontal gyri, cerebellar vermis and hemispheres, and cingulate and fusiform gyri. Nevertheless, TBM found additional volume reductions in the basal ganglia and the thalamus, while unmodulated VBM detected reduced gray matter density in the parahippocampal gyri bilaterally. The unmodulated, or standard VBM method measures the voxel intensity of smoothed, spatially normalized gray matter maps, which is defined as the locally weighted average of gray matter density in a region defined by a smoothing filter (Ashburner and Friston, 2000; Good et al., 2001b). If no modulation step is applied, comparisons of gray matter density alone do not fully reflect volume differences between subjects, as they do not contain information on the expansions and contractions needed to match the subject to the template (the Jacobian maps). The modulated, or optimized VBM method (Good et al., 2001b) addresses this issue by multiplying

(modulating) the voxel intensity value of the spatially normalized gray matter maps by the corresponding Jacobian determinant of the deformation fields, so that the measured amount of gray matter at each voxel, which is the product of the gray matter density and the volume of the deformed voxel, remains unchanged during warping. Davatzikos et al. (2001) have proposed a conceptually related approach. Nevertheless, if gray matter density and volumetric expansion are multiplied, the resulting compound measure at each voxel represents the mixed influence of regional gray matter volume, thickness and volumetric averaging by the smoothing filter (Eckert et al., 2006a), and thus may be somewhat less explicit in its physical meaning than using the Jacobian maps directly, which measure volume differences.

Based on comparing the ratio of verbal–performance IQ difference to the average of both test scores, the intellectual ability in WS subjects is more skewed toward language than visuospatial processing, compared with normal individuals. This is also evident in their relative facility in grammar, proclivity for unusual vocabulary, and enrichment in language affect, which is remarkable given their impairments in general cognition (Bellugi et al., 1999, 2001). Performance IQ in WS subjects aged 30 or over was found to be related to the volume of brain structures that have been previously reported to correlate with full-scale or performance IQ, such as prefrontal, parietal and occipital regions (Reiss et al., 1996; Flashman et al., 1997; Nguyen and McDaniel, 2000; Thompson et al., 2001; Posthuma et al., 2002; Gray and Thompson, 2004; Haier et al., 2004; McDaniel, 2005; Shaw et al., 2006). This may reflect a possible benefit of greater gray and/or white volume for visuospatial processing (perhaps via increased myelination or conduction velocity). The linkage of performance IQ with volumes of limbic structures, such as anterior cingulate gyrus, amygdala, hippocampus, and orbito-frontal areas may be of special interest. The anterior cingulate gyrus, particularly the dorsal part, is an important component of parallel distributed attentional and emotional networks that are involved in cognitive processing by handling conflicting or competitive stimuli coming from different brain areas (Bush et al., 2000). Its gray matter volume is also correlated with performance IQ (Wilke et al., 2003), although it is not clear whether this is an anatomically specific correlation or mediated by the overall relationship between brain volume and IQ. The right hippocampus is activated in topographical learning and memory retrieval tasks, showing increased regional blood flow on positron emission tomography (Maguire et al., 1996; Maguire, 1997; Meyer-Lindenberg et al., 2005b). Nevertheless, the mechanisms that associate brain structure volumes and intellectual ability, especially in the presence of disease interactions such as Williams syndrome, remain largely unknown. Alternatively, regions with positive correlations between performance IQ and brain volume may coincide with those that show significant volume differences between WS and controls. In that case, a greater relative preservation in brain volume may indicate less disease burden, and thus better intellectual performance. It is not surprising that we found no correlation between IQ and overall or regional brain volume for the whole WS or control group, as a large sample size is commonly required to detect such correlation in normal subjects (Nguyen and McDaniel, 2000; Thompson et al., 2001; Gray and Thompson, 2004), and the pattern of correlation may be different in different age groups (Wilke et al., 2003; Shaw et al., 2006). We also cannot rule out that there is an IQ \times disease interaction, but there were not enough control subjects with IQ scores available to determine this.

The results from our analysis of brain asymmetry showed the well-known frontal and occipital petalia in control subjects, consistent with other VBM studies (Good et al., 2001a; Watkins et al., 2001). To our knowledge, this asymmetry pattern has not been mapped before with TBM. WS subjects exhibited frontal petalia, but the occipital petalia was somewhat less prominent (albeit not significantly so). Prior volumetric analyses on this subject population showed a significant group \times side interaction with leftward asymmetry for occipital gray matter volume in WS subjects (Reiss et al., 2004); however, our TBM study did not detect this. Possible reasons include (i) TBM is less sensitive in detecting the relative extent of gray/white matter volume contributions; (ii) intensity-based registration may not match cortical gray matter as well as subcortical gray or white matter. In the normal population, the *planum temporale* is greater in volume in the left hemisphere (Geschwind and Levitsky, 1968; Galaburda et al., 1978; Good et al., 2001a; Watkins et al., 2001), although some reports found that such leftward asymmetry was not significant, which may be due to different anatomical criteria and parcellation methods, measurement of surface area rather than gray matter volume, power limitations in small samples, and the effects of brain size correction (Beaton, 1997; Westbury et al., 1999). Moreover, *planum temporale* is somewhat difficult to localize consistently on brain MRI and there is substantial volume variation and some cytoarchitectural variation of the histologically defined *planum temporale* with respect to grossly observable anatomical landmarks (Steinmetz et al., 1989). In WS subjects, we found that the right *planum temporale* was larger in volume, which is at variance with the leftward asymmetry in surface areas detected in a largely overlapping sample of subjects (Eckert et al., 2006b), and in a previous small-sample study (Hickok et al., 1995). This discrepancy may result from: (i) the volume comparison computed from the Jacobian determinant of registration deformation fields differing in definition from the volume or surface area measured in volumetric analysis; (ii) adjustment for overall brain volume by mapping data to the ICBM stereotaxic space may not have the same effect as linear detrending of the overall volume using statistical procedures such as ANCOVA; and (iii) intensity-based registration accuracy may be not optimal for small substructures such as the *planum temporale*, which lack sharply contrasting boundaries on MRI. Nevertheless, the leftward asymmetry in WS subjects was greatly reduced, and WS subjects had a significantly larger right *planum temporale*, but not left *planum temporale*, than the control subjects, whether the *planum* areas were adjusted for cerebral tissue volume or not (Eckert et al., 2006b). This may be linked with the thickening in the language cortex of the right hemisphere found in our previous study (Thompson et al., 2005).

In this paper, we used the “minimum-deformation target” (MDT) as the common template for image registration and

statistical comparisons, which is helpful to reduce any bias in the registration process towards the particular geometry of a single subject. We built the MDT by averaging the deformation fields rather than averaging the voxel intensities of the registered images (Evans et al., 1992; Good et al., 2001a; Watkins et al., 2001), as the effect sizes for group comparisons based on using an MDT with intensity distributions similar to a single brain have been found to be greater than using an average intensity atlas (Chiang et al., 2007). This is apparent in the subcortical gray matter where the intensity contrast with the surrounding white matter is lower when using an average intensity template. The MDT was derived from the best individual target (BIT) with lowest TQS among all study participants, which we considered as a better target than any individual subject because the geometry of the BIT is the most representative of the whole group and deviates the least from all other brains; i.e., the warping required for other subjects to be mapped to the BIT is minimal on average. Furthermore, using the BIT to make the MDT may be theoretically better than using a single-subject standard template, e.g., the Colin27 brain template (Holmes et al., 1998), as in our previous approach (Lee et al., 2007), as the BIT was scanned with the same imaging parameters and has a similar morphology to the study subjects. Nevertheless, the BIT–MDT method suffers from a relatively high computational load (it requires $N(N-1)$ or $\sim N^2$ nonlinear registrations for N subjects to determine the BIT), and further comparisons of these two approaches on the effect sizes for disease detection are required (see Chou et al., 2007 for related work).

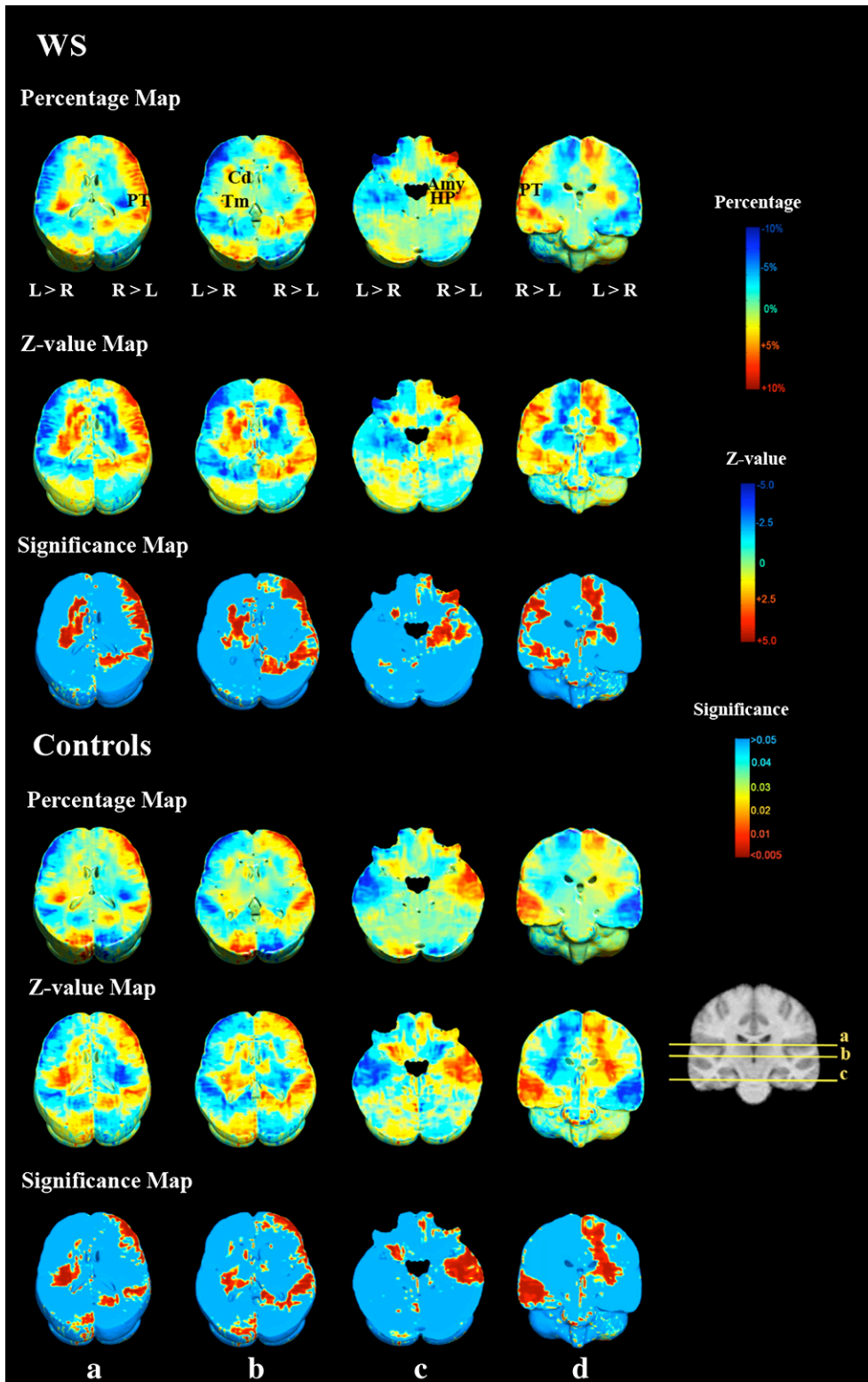
Prior to nonlinear deformation, all images were first aligned to the ICBM template using affine registration with scaling in x -, y -, and z -directions, such that the linear term was fitted before estimating the nonlinear parameters. Although the warping can be performed on the native space data, an initial 9-parameter transformation helps to avoid misregistrations due to the deformation field settling in local minima of the cost function, and to accelerate convergence. J_{ICBM} obtained from fluid mapping in the ICBM space for an individual subject to the MDT is then convertible to J_{native} in the native space by dividing by the zoom factor resulting from the affine transformation. Comparing J_{ICBM} can be considered as comparing the relative (proportional) volumes of regional brain structures, as the difference in global brain volume has been scaled out, while J_{native} refers to the regional volume of structures at their original scale (native space or ‘scanner space’). We studied brain asymmetry using J_{ICBM} in order to avoid giving greater weights on more-symmetric brains with greater global volume in statistical tests than more-asymmetric ones with smaller global volume. This also ensured that regional differences were not confounded by global brain differences when group \times side interactions are tested. On the other hand, we linked J_{native} with IQ scores, as we were interested in detecting the specific regions where their native volume is positively

Fig. 5. Visualization of the brain asymmetry pattern in WS subjects and controls. In each group, the percentage maps (showing relative volume) were computed based on the difference in the $\log(J_{ICBM})$ between the ipsilateral voxel and its mirror image (with respect to the midsagittal plane) in the contralateral hemisphere, with an asymmetry percentage value defined as $100\% \times (J_L - J_R) / [(J_L + J_R) / 2]$ for voxels in the left hemisphere, and $100\% \times (J_R - J_L) / [(J_L + J_R) / 2]$ for voxels in the right hemisphere, where J_R and J_L are the corresponding Jacobian determinants in left and right hemispheres (Steinmetz, 1996). The difference in the $\log(J_{ICBM})$ between left and right sides was tested nonparametrically to obtain z -value maps using the normal approximation to the Mann–Whitney distribution, with $z > 0$ indicating ipsilateral $>$ contralateral, color-coded in red, and $z < 0$ for ipsilateral $<$ contralateral, color-coded in blue. The z -value maps are associated with probability maps that indicate the significance of z -values greater than zero. Both WS and control subjects exhibited frontal and occipital petalias (rightward asymmetry in frontal and temporal lobes, and leftward asymmetry in occipital lobes), though the occipital petalia was less apparent in WS. The thalamus, putamen, globus pallidus, and caudate nucleus were larger in the left hemisphere in both groups. The *planum temporale* was larger in the right hemisphere in WS subjects, but larger in the left hemisphere in control subjects. Even so, this difference was either at trend-level or only significant in the medial part. Compared with control subjects, WS participants showed a trend for a larger right amygdala and hippocampus, but this group-by-side interaction did not reach statistical significance when formally tested by ANOVA. Abbreviations: Amy: amygdala, Cd: caudate nucleus, HP: hippocampus, PT: planum temporale, Tm: thalamus.

correlated to subjects' IQ, on the basis that greater total brain volume is correlated with higher IQ and may be functionally beneficial for physiological reasons (McDaniel, 2005).

Although this study, as well as others (Schmitt et al., 2001b; Meyer-Lindenberg et al., 2004; Reiss et al., 2004), suggests a

seemingly natural rule that reduction and preservation of volume may be linked with the functional integrity or capacity of brain structures in WS and normal subjects, this may imply an overly simplistic relationship between structure and function. For instance, increased thickness in the perisylvian region of the parieto-occipital



cortex in WS was not clearly associated with any apparent functional gain but mostly likely with aberrant packing of cortical neurons (Thompson et al., 2005). A combined VBM and functional MRI study on WS subjects revealed that even though the volume of the hippocampal formation was preserved, its function was impaired (Meyer-Lindenberg et al., 2005b). To understand relations between white matter volume and its functional integrity, different types of investigations are required. A preliminary diffusion tensor imaging study showed reduced diffusivity indices (fractional anisotropy and trace) in the right parieto-occipital regions, indicating altered white matter integrity (Marenco et al., 2004). We expect that a future combination of TBM and diffusion tensor imaging will be advantageous in unraveling the underlying white-matter structural–functional connection in WS.

Acknowledgments

This work was funded by grants from the National Institute for Biomedical Imaging and Bioengineering, the National Center for Research Resources, and the National Institute on Aging, (EB01651, RR019771, AG016570 to PT), from the National Institute of Mental Health (K02 MH01142; to ALR), and the National Institute of Child Health and Human Development (R01 HD31715 to ALR and P01 HD33113 to ALR, JRK, DM, AG and UB). Additional support was provided by NCRR Resource grant P41 RR13642 to AWT, and a fellowship from the Government of Taiwan (to M.C.C.).

Appendix A. Analysis of covariance for the group difference of regional brain volume

To detrend any possible confounding effect of subjects' age on the regional volumetric differences observed between groups, analysis of covariance was performed at each voxel by least-squares fitting of coefficients β_i in the following general linear model:

$$\log(J_{ICBM}) = \beta_0 + \beta_1 \cdot \text{Diagnosis} + \beta_2 \cdot \text{Age} + \varepsilon. \quad (\text{A1})$$

Here diagnosis was coded as a binary variable (0 for control and 1 for WS), and age was detrended as a covariate. ε is an error term. We then tested $H_0: \beta_1 = 0$ by defining an F statistic (Rencher, 2002), distributed approximately as $F_{h,n-q-1}$:

$$F = \frac{(\text{SSR}_f - \text{SSR}_r)/h}{\text{SSE}_f/(n-q-1)}, \quad (\text{A2})$$

where $\text{SSR}_f = \sum_{i=1}^n \sum_{j=0}^q \hat{\beta}_j x_{ij} y_i$ is the regression sum of squares, and

$$\text{SSE}_f = \sum_{i=1}^n \left(y_i - \sum_{j=0}^q \hat{\beta}_j x_{ij} \right)^2$$

is the sum of squares of error for the full model (Eq. (A1)). $\text{SSR}_r = \sum_{i=1}^n \sum_{j=0}^{q-h} \hat{\beta}_{rj} x_{rj} y_i$ is the regression sum of squares for the reduced model:

$$\log(J_{ICBM}) = \beta_{r0} + \beta_{r1} \cdot \text{Age} + \varepsilon_r. \quad (\text{A3})$$

Here n is the total number of subjects, q is the number of variables in the full model (=2 for diagnosis and age), and h is the number of variable to be tested (=1 for diagnosis). y_i represents $\log(J_{ICBM})$, $\hat{\beta}_j$ or $\hat{\beta}_{rj}$ the estimated regression coefficient, and x_{ij} or x_{rj}

the independent variables of subject i , with the subscript r for the reduced model; for instance, x_{i1} indicates the value coding for diagnosis (0 or 1), and x_{i2} the age of subject i , and $x_{i0}=1$ is the regression constant. We rejected H_0 if $F > F_{\alpha}$, where $\alpha=0.01$.

Appendix B. Repeated measures analysis of variance for the group by side interaction effect

We compared the difference in asymmetry between WS and control groups by voxelwise testing the following null hypothesis H_0 :

$$\mu_{00} - \mu_{01} = \mu_{10} - \mu_{11}, \quad (\text{B1})$$

where μ_{ij} is the mean of $\log(J_{ICBM})$ at the voxel for diagnosis group i and side j , with $i \in \{0,1\} = \{\text{control, WS}\}$ and $j \in \{0,1\} = \{\text{left, right}\}$. Writing Eq. (B1) in matrix–vector form, we defined a contrast vector $\mathbf{c} = [1 - 1]^T$, then the above H_0 becomes:

$$\mathbf{c}^T \boldsymbol{\mu}_0 = \mathbf{c}^T \boldsymbol{\mu}_1, \quad (\text{B2})$$

where $\boldsymbol{\mu}_i = [\mu_{i0} \ \mu_{i1}]^T$. The group \times side interaction effect can be tested by the Wilks' Λ (Rencher, 2002):

$$\Lambda = \frac{|\mathbf{c}^T \mathbf{E} \mathbf{c}|}{|\mathbf{c}^T (\mathbf{E} + \mathbf{H}) \mathbf{c}|}. \quad (\text{B3})$$

Here $\mathbf{E} = \sum_{k=0}^{K-1} \sum_{l=0}^{n_k-1} (\mathbf{y}_{kl} - \bar{\mathbf{y}}_{k\cdot})(\mathbf{y}_{kl} - \bar{\mathbf{y}}_{k\cdot})^T$ and $\mathbf{H} = \sum_{k=0}^{K-1} n_k (\bar{\mathbf{y}}_{k\cdot} - \bar{\mathbf{y}}_{\cdot\cdot})(\bar{\mathbf{y}}_{k\cdot} - \bar{\mathbf{y}}_{\cdot\cdot})^T$ is the voxel value vector for $\log(J_{ICBM})$ at the left (subscript=0) and right (subscript=1) sides of subject l in diagnosis group k , $\bar{\mathbf{y}}_{k\cdot} = \sum_{l=0}^{n_k-1} \mathbf{y}_{kl}/n_k$, and $\bar{\mathbf{y}}_{\cdot\cdot} = \sum_{k=0}^{K-1} \sum_{l=0}^{n_k-1} \mathbf{y}_{kl}/N$, while $N = \sum_{k=0}^{K-1} n_k$ is the total number of subjects, which were assigned to K diagnostic groups with each group composed of n_k subjects. Λ is distributed as $\Lambda_{p,vH,vE}$, with p =number of sides (left and right) $-1=1$, $vH=K-1$, and $vE=N-K$. We rejected H_0 if $\Lambda \leq \Lambda_{\alpha,p,vH,vE}$, where α was set to 0.01.

References

- Arsigny, V., Fillard, P., Pennec, X., Ayache, N., 2005. Fast and simple calculus on tensors in the log-Euclidean framework. Int. Conf. Med. Image Comput. Comput. Assist. Interv. (MICCAI), pp. 115–122.
- Ashburner, J., Friston, K.J., 2000. Voxel-based morphometry—the methods. NeuroImage 11, 805–821.
- Avants, B., Gee, J.C., 2004. Geodesic estimation for large deformation anatomical shape averaging and interpolation. NeuroImage 23 (Suppl. 1), S139–S150.
- Avants, B.B., Schoenemann, P.T., Gee, J.C., 2006. Lagrangian frame diffeomorphic image registration: morphometric comparison of human and chimpanzee cortex. Med. Image Anal. 10, 397–412.
- Beaton, A.A., 1997. The relation of planum temporale asymmetry and morphology of the corpus callosum to handedness, gender, and dyslexia: a review of the evidence. Brain Lang. 60, 255–322.
- Bellugi, U., Lichtenberger, L., Mills, D., Galaburda, A., Korenberg, J.R., 1999. Bridging cognition, the brain and molecular genetics: evidence from Williams syndrome. Trends Neurosci. 22, 197–207.
- Bellugi, U., Lichtenberger, L., Jones, W., Lai, Z., St. George, M., 2000. I. The neurocognitive profile of Williams syndrome: a complex pattern of strengths and weaknesses. J. Cogn. Neurosci. 12 (Suppl. 1), 7–29.
- Bellugi, U., Korenberg, J.R., Klima, E.S., 2001. Williams syndrome: an exploration of neurocognitive and genetic features. Clin. Neurosci. Res. 1, 217–229.

- Benjamini, Y., Hochberg, Y., 1995. Controlling the false discovery rate: a practical and powerful approach to multiple testing. *J. R. Stat. Soc. Ser. B., Methodol.* 57, 289–300.
- Boddaert, N., Mochel, F., Meresse, I., Seidenwurm, D., Cachia, A., Brunelle, F., Lyonnet, S., Zilbovicius, M., 2006. Parieto-occipital grey matter abnormalities in children with Williams syndrome. *NeuroImage* 30, 721–725.
- Brown, J.H., Johnson, M.H., Paterson, S.J., Gilmore, R., Longhi, E., Karmiloff-Smith, A., 2003. Spatial representation and attention in toddlers with Williams syndrome and Down syndrome. *Neuropsychologia* 41, 1037–1046.
- Bush, G., Luu, P., Posner, M.I., 2000. Cognitive and emotional influences in anterior cingulate cortex. *Trends Cogn. Sci.* 4, 215–222.
- Carrion, V.G., Weems, C.F., Eliez, S., Patwardhan, A., Brown, W., Ray, R.D., Reiss, A.L., 2001. Attenuation of frontal asymmetry in pediatric posttraumatic stress disorder. *Biol. Psychiatry* 50, 943–951.
- Chiang, M.-C., Dutton, R.A., Hayashi, K.M., Lopez, O.L., Aizenstein, H.J., Toga, A.W., Becker, J.T., Thompson, P.M., 2007. 3D pattern of brain atrophy in HIV/AIDS visualized using tensor-based morphometry. *NeuroImage* 34, 44–60.
- Chou, Y., Leporé, N., de Zubicaray, G., Rose, S., Carmichael, O., Becker, J., Toga, A., Thompson, P., 2007. Automatic 3D mapping and analysis of the lateral ventricles using fluid registration of multiple labeled atlases. *IEEE International Symposium on Biomedical Imaging: From Nano to Macro (ISBI)*.
- Christensen, G.E., Johnson, H.J., 2001. Consistent image registration. *IEEE Trans. Med. Imag.* 20, 568–582.
- Christensen, G.E., Johnson, H.J., Vannier, M.W., 2006. Synthesizing average 3D anatomical shapes. *NeuroImage* 32, 146–158.
- Chung, M.K., Worsley, K.J., Paus, T., Cherif, C., Collins, D.L., Giedd, J.N., Rapoport, J.L., Evans, A.C., 2001. A unified statistical approach to deformation-based morphometry. *NeuroImage* 14, 595–606.
- Chung, M.K., Dalton, K.M., Alexander, A.L., Davidson, R.J., 2004. Less white matter concentration in autism: 2D voxel-based morphometry. *NeuroImage* 23, 242–251.
- Collins, D.L., Holmes, C.J., Peters, T.M., Evans, A.C., 1995. Automatic 3-D model-based neuroanatomical segmentation. *Hum. Brain Mapp.* 3, 190–208.
- Davatzikos, C., Vaillant, M., Resnick, S.M., Prince, J.L., Letovsky, S., Bryan, R.N., 1996. A computerized approach for morphological analysis of the corpus callosum. *J. Comput. Assist. Tomogr.* 20, 88–97.
- Davatzikos, C., Genc, A., Xu, D., Resnick, S.M., 2001. Voxel-based morphometry using the RAVENS maps: methods and validation using simulated longitudinal atrophy. *NeuroImage* 14, 1361–1369.
- de Lacoste, M.C., Kirkpatrick, J.B., Ross, E.D., 1985. Topography of the human corpus callosum. *J. Neuropathol. Exp. Neurol.* 44, 578–591.
- Eckert, M.A., Hu, D., Eliez, S., Bellugi, U., Galaburda, A., Korenberg, J., Mills, D., Reiss, A.L., 2005. Evidence for superior parietal impairment in Williams syndrome. *Neurology* 64, 152–153.
- Eckert, M.A., Tenforde, A., Galaburda, A.M., Bellugi, U., Korenberg, J.R., Mills, D., Reiss, A.L., 2006a. To modulate or not to modulate: differing results in uniquely shaped Williams syndrome brains. *NeuroImage* 32, 1001–1007.
- Eckert, M.A., Galaburda, A.M., Karchemskiy, A., Liang, A., Thompson, P., Dutton, R.A., Lee, A.D., Bellugi, U., Korenberg, J.R., Mills, D., Rose, F.E., Reiss, A.L., 2006b. Anomalous sylvian fissure morphology in Williams syndrome. *NeuroImage* 33, 39–45.
- Edgington, E.S., 1995. *Randomization Tests*. Marcel Dekker, New York, NY.
- Evans, A.C., Collins, D.L., Milner, B., 1992. An MRI-based stereotactic brain atlas from 300 young normal subjects. *Proc. 22nd Annu. Symp. Soc. Neurosci. Anaheim*, p. 408.
- Fischl, B., Sereno, M.I., Tootell, R.B., Dale, A.M., 1999. High-resolution intersubject averaging and a coordinate system for the cortical surface. *Hum. Brain Mapp.* 8, 272–284.
- Flashman, L.A., Andreasen, N.C., Flaum, M., 1997. Intelligence and regional brain volumes in normal controls. *Intelligence* 25, 149–160.
- Fox, N.C., Crum, W.R., Scahill, R.I., Stevens, J.M., Janssen, J.C., Rossor, M.N., 2001. Imaging of onset and progression of Alzheimer's disease with voxel-compression mapping of serial magnetic resonance images. *Lancet* 358, 201–205.
- Galaburda, A.M., LeMay, M., Kemper, T.L., Geschwind, N., 1978. Right-left asymmetries in the brain. *Science* 199, 852–856.
- Gaser, C., Luders, E., Thompson, P.M., Lee, A.D., Dutton, R.A., Geaga, J.A., Hayashi, K.M., Bellugi, U., Galaburda, A.M., Korenberg, J.R., Mills, D.L., Toga, A.W., Reiss, A.L., 2006. Increased local gyrification mapped in Williams syndrome. *NeuroImage* 33, 46–54.
- Genovese, C.R., Lazar, N.A., Nichols, T., 2002. Thresholding of statistical maps in functional neuroimaging using the false discovery rate. *NeuroImage* 15, 870–878.
- Geschwind, N., Levitsky, W., 1968. Human brain: left-right asymmetries in temporal speech region. *Science* 161, 186–187.
- Good, C.D., Johnsrude, I., Ashburner, J., Henson, R.N., Friston, K.J., Frackowiak, R.S., 2001a. Cerebral asymmetry and the effects of sex and handedness on brain structure: a voxel-based morphometric analysis of 465 normal adult human brains. *NeuroImage* 14, 685–700.
- Good, C.D., Johnsrude, I.S., Ashburner, J., Henson, R.N., Friston, K.J., Frackowiak, R.S., 2001b. A voxel-based morphometric study of ageing in 465 normal adult human brains. *NeuroImage* 14, 21–36.
- Gray, J.R., Thompson, P.M., 2004. Neurobiology of intelligence: science and ethics. *Nat. Rev., Neurosci.* 5, 471–482.
- Haier, R.J., Jung, R.E., Yeo, R.A., Head, K., Alkire, M.T., 2004. Structural brain variation and general intelligence. *NeuroImage* 23, 425–433.
- Haxby, J.V., 2006. Fine structure in representations of faces and objects. *Nat. Neurosci.* 9, 1084–1086.
- Haxby, J.V., Ungerleider, L.G., Clark, V.P., Schouten, J.L., Hoffman, E.A., Martin, A., 1999. The effect of face inversion on activity in human neural systems for face and object perception. *Neuron* 22, 189–199.
- Hickok, G., Bellugi, U., Jones, W., 1995. Asymmetrical ability. *Science* 270, 219–220.
- Hoffman, E.A., Haxby, J.V., 2000. Distinct representations of eye gaze and identity in the distributed human neural system for face perception. *Nat. Neurosci.* 3, 80–84.
- Holmes, C.J., Hoge, R., Collins, L., Woods, R., Toga, A.W., Evans, A.C., 1998. Enhancement of MR images using registration for signal averaging. *J. Comput. Assist. Tomogr.* 22, 324–333.
- Jernigan, T.L., Bellugi, U., Sowell, E., Doherty, S., Hesselink, J.R., 1993. Cerebral morphologic distinctions between Williams and Down syndromes. *Arch. Neurol.* 50, 186–191.
- Joshi, S., Davis, B., Jomier, M., Gerig, G., 2004. Unbiased diffeomorphic atlas construction for computational anatomy. *NeuroImage* 23 (Suppl. 1), S151–S160.
- Kawashima, R., Sugiura, M., Kato, T., Nakamura, A., Hatano, K., Ito, K., Fukuda, H., Kojima, S., Nakamura, K., 1999. The human amygdala plays an important role in gaze monitoring. A PET study. *Brain* 122 (Pt. 4), 779–783.
- Kochunov, P., Lancaster, J.L., Thompson, P., Woods, R., Mazziotta, J., Hardies, J., Fox, P., 2001. Regional spatial normalization: toward an optimal target. *J. Comput. Assist. Tomogr.* 25, 805–816.
- Korenberg, J.R., Chen, X.N., Hirota, H., Lai, Z., Bellugi, U., Burian, D., Roe, B., Matsuoka, R., 2000. VI. Genome structure and cognitive map of Williams syndrome. *J. Cogn. Neurosci.* 12 (Suppl. 1), 89–107.
- Lee, A.D., Leow, A.D., Lu, A., Reiss, A.L., Hall, S., Chiang, M.C., Toga, A.W., Thompson, P.M., 2007. 3D pattern of brain abnormalities in Fragile X syndrome visualized using tensor-based morphometry. *NeuroImage* 34, 924–938.
- Leow, A., Huang, S., Geng, A., Becker, J., Davis, S., Toga, A., Thompson, P., 2005. Inverse consistent mapping in 3D deformable image registration: its construction and statistical properties. *Information Processing in Medical Imaging (IPMI)*. Glenwood Springs, Colorado.
- Leow, A.D., Klunder, A.D., Jack Jr., C.R., Toga, A.W., Dale, A.M., Bernstein, M.A., Britson, P.J., Gunter, J.L., Ward, C.P., Whitwell, J.L., Borowski, B.J., Fleisher, A.S., Fox, N.C., Harvey, D., Kornak, J.,

- Schuff, N., Studholme, C., Alexander, G.E., Weiner, M.W., Thompson, P.M., 2006. Longitudinal stability of MRI for mapping brain change using tensor-based morphometry. *NeuroImage* 31, 627–640.
- Levitin, D.J., Menon, V., Schmitt, J.E., Eliez, S., White, C.D., Glover, G.H., Kadis, J., Korenberg, J.R., Bellugi, U., Reiss, A.L., 2003. Neural correlates of auditory perception in Williams syndrome: an fMRI study. *NeuroImage* 18, 74–82.
- Lui, L.M., Wang, Y., Chan, T.F., Thompson, P.M., 2007. Brain anatomical feature detection by solving partial differential equations on a general manifold. *J. Discrete Cont. Dyn. Syst., Ser. B* 7, 605–618.
- Maguire, E.A., 1997. Hippocampal involvement in human topographical memory: evidence from functional imaging. *Philos. Trans. R. Soc. Lond., B Biol. Sci.* 352, 1475–1480.
- Maguire, E.A., Frackowiak, R.S., Frith, C.D., 1996. Learning to find your way: a role for the human hippocampal formation. *Proc. Biol. Sci.* 263, 1745–1750.
- Manly, K.F., Nettleton, D., Hwang, J.T., 2004. Genomics, prior probability, and statistical tests of multiple hypotheses. *Genome Res.* 14, 997–1001.
- Marenco, S., Meyer-Lindberg, A., Kippenhan, S., Olsen, R.K., Mervis, C.B., Morris, C.A., Pierpaoli, C., Berman, K.F., 2004. Preliminary diffusion tensor imaging (DTI) observations in 5 individuals with Williams syndrome (WS). *Human Brain Mapping*. Budapest, Hungary.
- Mazziotta, J., Toga, A., Evans, A., Fox, P., Lancaster, J., Zilles, K., Woods, R., Paus, T., Simpson, G., Pike, B., Holmes, C., Collins, L., Thompson, P., MacDonald, D., Iacoboni, M., Schormann, T., Amunts, K., Palomero-Gallagher, N., Geyer, S., Parsons, L., Narr, K., Kabani, N., Le Goualher, G., Boomsma, D., Cannon, T., Kawashima, R., Mazoyer, B., 2001. A probabilistic atlas and reference system for the human brain: International Consortium for Brain Mapping (ICBM). *Philos. Trans. R. Soc. Lond., B Biol. Sci.* 356, 1293–1322.
- McDaniel, M.A., 2005. Big-brained people are smarter: a meta-analysis of the relationship between in vivo brain volume and intelligence. *Intelligence* 33, 337–346.
- Meyer-Lindenberg, A., Kohn, P., Mervis, C.B., Kippenhan, J.S., Olsen, R.K., Morris, C.A., Berman, K.F., 2004. Neural basis of genetically determined visuospatial construction deficit in Williams syndrome. *Neuron* 43, 623–631.
- Meyer-Lindenberg, A., Hariri, A.R., Munoz, K.E., Mervis, C.B., Mattay, V.S., Morris, C.A., Berman, K.F., 2005a. Neural correlates of genetically abnormal social cognition in Williams syndrome. *Nat. Neurosci.* 8, 991–993.
- Meyer-Lindenberg, A., Mervis, C.B., Sarpal, D., Koch, P., Steele, S., Kohn, P., Marenco, S., Morris, C.A., Das, S., Kippenhan, S., Mattay, V.S., Weinberger, D.R., Berman, K.F., 2005b. Functional, structural, and metabolic abnormalities of the hippocampal formation in Williams syndrome. *J. Clin. Invest.* 115, 1888–1895.
- Mobbs, D., Garrett, A.S., Menon, V., Rose, F.E., Bellugi, U., Reiss, A.L., 2004. Anomalous brain activation during face and gaze processing in Williams syndrome. *Neurology* 62, 2070–2076.
- Mobbs, D., Eckert, M.A., Mills, D., Korenberg, J., Bellugi, U., Galaburda, A.M., Reiss, A.L., 2006. Frontostriatal dysfunction during response inhibition in Williams syndrome. *Biol. Psychiatry*.
- Nguyen, N.T., McDaniel, M.A., 2000. Brain size and intelligence: a meta-analysis. *First Annual Conference of the International Society of Intelligence Research*, Cleveland, OH.
- Nichols, T.E., Holmes, A.P., 2001. Nonparametric permutation tests for functional neuroimaging: a primer with examples. *Hum. Brain Mapp.* 15, 1–25.
- Park, H.J., Kubicki, M., Shenton, M.E., Guimond, A., McCarley, R.W., Maier, S.E., Kikinis, R., Jolesz, F.A., Westin, C.F., 2003. Spatial normalization of diffusion tensor MRI using multiple channels. *NeuroImage* 20, 1995–2009.
- Park, H.J., Westin, C.F., Kubicki, M., Maier, S.E., Niznikiewicz, M., Baer, A., Frumin, M., Kikinis, R., Jolesz, F.A., McCarley, R.W., Shenton, M.E., 2004. White matter hemisphere asymmetries in healthy subjects and in schizophrenia: a diffusion tensor MRI study. *NeuroImage* 23, 213–223.
- Posthuma, D., De Geus, E.J., Baare, W.F., Hulshoff Pol, H.E., Kahn, R.S., Boomsma, D.I., 2002. The association between brain volume and intelligence is of genetic origin. *Nat. Neurosci.* 5, 83–84.
- Reiss, A.L., Abrams, M.T., Singer, H.S., Ross, J.L., Denckla, M.B., 1996. Brain development, gender and IQ in children. A volumetric imaging study. *Brain* 119 (Pt. 5), 1763–1774.
- Reiss, A.L., Eliez, S., Schmitt, J.E., Straus, E., Lai, Z., Jones, W., Bellugi, U., 2000. IV. Neuroanatomy of Williams syndrome: a high-resolution MRI study. *J. Cogn. Neurosci.* 12 (Suppl. 1), 65–73.
- Reiss, A.L., Eckert, M.A., Rose, F.E., Karchemskiy, A., Kesler, S., Chang, M., Reynolds, M.F., Kwon, H., Galaburda, A., 2004. An experiment of nature: brain anatomy parallels cognition and behavior in Williams syndrome. *J. Neurosci.* 24, 5009–5015.
- Rencher, A.C., 2002. *Methods of Multivariate Analysis*, 2nd edition. J. Wiley, New York.
- Schmitt, J.E., Eliez, S., Warsofsky, I.S., Bellugi, U., Reiss, A.L., 2001a. Enlarged cerebellar vermis in Williams syndrome. *J. Psychiatr. Res.* 35, 225–229.
- Schmitt, J.E., Eliez, S., Warsofsky, I.S., Bellugi, U., Reiss, A.L., 2001b. Corpus callosum morphology of Williams syndrome: relation to genetics and behavior. *Dev. Med. Child Neurol.* 43, 155–159.
- Shattuck, D.W., Leahy, R.M., 2002. BrainSuite: an automated cortical surface identification tool. *Med. Image Anal.* 6, 129–142.
- Shaw, P., Greenstein, D., Lerch, J., Clasen, L., Lenroot, R., Gogtay, N., Evans, A., Rapoport, J., Giedd, J., 2006. Intellectual ability and cortical development in children and adolescents. *Nature* 440, 676–679.
- Shen, D., Davatzikos, C., 2003. Very high-resolution morphometry using mass-preserving deformations and HAMMER elastic registration. *NeuroImage* 18, 28–41.
- Shi, Y., Reiss, A., Lee, A., Dutton, R., Bellugi, U., Galaburda, A., Korenberg, J., Mills, D., Dinov, I., Thompson, P., Toga, A., 2007. Hamilton–Jacobi skeletons on cortical surfaces with applications in characterizing the gyrification pattern in Williams syndrome. *IEEE International Symposium on Biomedical Imaging: From Nano to Macro (ISBI)*.
- Steinmetz, H., 1996. Structure, functional and cerebral asymmetry: in vivo morphometry of the planum temporale. *Neurosci. Biobehav. Rev.* 20, 587–591.
- Steinmetz, H., Rademacher, J., Huang, Y.X., Hefter, H., Zilles, K., Thron, A., Freund, H.J., 1989. Cerebral asymmetry: MR planimetry of the human planum temporale. *J. Comput. Assist. Tomogr.* 13, 996–1005.
- Storey, J.D., 2002. A direct approach to false discovery rates. *J. R. Stat. Soc., Ser. B Stat. Methodol.* 64, 479–498.
- Storey, J.D., Tibshirani, R., 2001. Estimating false discovery rates under dependence, with applications to DNA microarrays. *Technical Report 2001-28*, Department of Statistics, Stanford University.
- Studholme, C., Cardenas, V., 2004. A template free approach to volumetric spatial normalization of brain anatomy. *Pattern Recogn. Lett.* 25, 1191–1202.
- Studholme, C., Cardenas, V., Blumenfeld, R., Schuff, N., Rosen, H.J., Miller, B., Weiner, M., 2004. Deformation tensor morphometry of semantic dementia with quantitative validation. *NeuroImage* 21, 1387–1398.
- Thompson, P.M., Schwartz, C., Toga, A.W., 1996. High-resolution random mesh algorithms for creating a probabilistic 3D surface atlas of the human brain. *NeuroImage* 3, 19–34.
- Thompson, P.M., Giedd, J.N., Woods, R.P., MacDonald, D., Evans, A.C., Toga, A.W., 2000. Growth patterns in the developing brain detected by using continuum mechanical tensor maps. *Nature* 404, 190–193.
- Thompson, P.M., Cannon, T.D., Narr, K.L., van Erp, T., Poutanen, V.P., Huttunen, M., Lonnqvist, J., Standertskjold-Nordenstam, C.G., Kaprio, J., Khaledy, M., Dail, R., Zoumalan, C.I., Toga, A.W., 2001. Genetic influences on brain structure. *Nat. Neurosci.* 4, 1253–1258.
- Thompson, P.M., Lee, A.D., Dutton, R.A., Geaga, J.A., Hayashi, K.M., Eckert, M.A., Bellugi, U., Galaburda, A.M., Korenberg, J.R., Mills, D.L., Toga, A.W., Reiss, A.L., 2005. Abnormal cortical complexity and

- thickness profiles mapped in Williams syndrome. *J. Neurosci.* 25, 4146–4158.
- Toga, A.W., Thompson, P.M., 2003. Mapping brain asymmetry. *Nat. Rev., Neurosci.* 4, 37–48.
- Tomaiuolo, F., Di Paola, M., Caravale, B., Vicari, S., Petrides, M., Caltagirone, C., 2002. Morphology and morphometry of the corpus callosum in Williams syndrome: a T1-weighted MRI study. *NeuroReport* 13, 2281–2284.
- Tosun, D., Reiss, A., Lee, A., Dutton, R., Geaga, J., Hayashi, K., Eckert, M., Bellugi, U., Galaburda, A., Korenberg, J., Mills, D., Toga, A., Thompson, P., 2006. Use of 3-D cortical morphometry for mapping increased cortical gyrification and complexity in Williams syndrome. *IEEE International Symposium on Biomedical Imaging: From Nano to Macro (ISBI)*, Arlington, Virginia.
- Tosun, D., Reiss, A., Lee, A., Dutton, R., Bellugi, U., Galaburda, A., Korenberg, J., Mills, D., Toga, A., Thompson, P., 2007. Use of cortical curvature features to analyze local and regional cortical folding complexity. to be submitted to *NeuroImage*, Dec 2006.
- Twining, C.J., Cootes, T., Marsland, S., Petrovic, V., Schestowitz, R., Taylor, C.J., 2005. A unified information-theoretic approach to groupwise non-rigid registration and model building. *Information Processing in Medical Imaging: 19th International Conference, IPMI 2005*, pp. 1–14. Glenwood Springs, CO.
- Wang, Y., Chiang, M.C., Thompson, P.M., 2005. Automated surface matching using mutual information applied to Riemann surface structures. *Int Conf Med Image Comput Comput. Assist Interv (MICCAI)*. Palm Springs, CA, pp. 666–674.
- Watkins, K.E., Paus, T., Lerch, J.P., Zijdenbos, A., Collins, D.L., Neelin, P., Taylor, J., Worsley, K.J., Evans, A.C., 2001. Structural asymmetries in the human brain: a voxel-based statistical analysis of 142 MRI scans. *Cereb. Cortex* 11, 868–877.
- Westbury, C.F., Zatorre, R.J., Evans, A.C., 1999. Quantifying variability in the planum temporale: a probability map. *Cereb. Cortex* 9, 392–405.
- Wilke, M., Sohn, J.H., Byars, A.W., Holland, S.K., 2003. Bright spots: correlations of gray matter volume with IQ in a normal pediatric population. *NeuroImage* 20, 202–215.
- Woods, R.P., 2003. Characterizing volume and surface deformations in an atlas framework: theory, applications, and implementation. *NeuroImage* 18, 769–788.